Atmos. Meas. Tech. Discuss., 6, 6147–6186, 2013
www.atmos-meas-tech-discuss.net/6/6147/2013/
doi:10.5194/amtd-6-6147-2013

Atmospheric Measurement Techniques Discussions

Application of high resolution Chemical Ionization Mass Spectrometry (CI-ToFMS) to study SOA composition: focus on formation of oxygenated species via aqueous phase processing

D. Aljawhary, A. K. Y. Lee, and J. P. D. Abbatt

Department of Chemistry, University of Toronto, Toronto, ON Canada M5S 3H6, Canada

Received: 24 May 2013 – Accepted: 10 June 2013 – Published: 4 July 2013

Correspondence to: J. P. D. Abbatt (jabbatt@chem.utoronto.ca)

Published by Copernicus Publications on behalf of the European Geosciences Union.

Abstract

This paper demonstrates the capabilities of Chemical Ionization Mass Spectrometry (CIMS) to study secondary organic aerosol (SOA) composition with a high resolution (HR) time-of-flight mass analyzer (aerosol-CI-ToFMS). In particular, by studying aqueous oxidation of Water Soluble Organic Compounds (WSOC) extracted from α-pinene ozonolysis SOA, we assess the capabilities of three common CIMS reagent ions: (a) protonated water clusters $(H_2O)_nH^+$, (b) acetate $CH_3C(O)O^-$ and (c) iodide water clusters $I(H_2O)_n^-$ to monitor SOA composition. As well, we report the relative sensitivity of these reagent ions to a wide range of common organic aerosol constituents. We find that $(H_2O)_nH^+$ is more selective to the detection of less oxidized species, so that the range of O/C and OS_C (carbon oxidation state) in the SOA spectra is considerably lower than those measured using $CH_3C(O)O^-$ and $I(H_2O)_n^-$. Specifically, $(H_2O)_nH^+$ ionizes organic compounds with $OS_C \leq 1.3$, whereas $CH_3C(O)O^-$ and $I(H_2O)_n^-$ both ionize highly oxygenated organics with OS_C up to 4 with $I(H_2O)_n^-$ being more selective towards multi-functional organic compounds. In the bulk O/C and H/C space, i.e. in a Van Krevelen plot, there is a remarkable agreement in both absolute magnitude and oxidation trajectory between CI-ToFMS data and those from a high resolution aerosol mass spectrometer (HR-AMS). This indicates that the CI-ToFMS data captures much of the chemical change occurring in the particle and that gas phase species, which are not detected by the HR-AMS, do not dominate the overall ion signal. Finally, the data illustrate the capability of aerosol-CI-ToFMS to monitor specific chemical change, including the fragmentation and functionalization reactions that occur during organic oxidation, and the oxidative conversion of dimeric SOA species into monomers. Overall, aerosol-CI-ToFMS is a valuable, selective complement to some common SOA characterization methods, such as AMS and spectroscopic techniques. Both laboratory and ambient SOA samples can be analyzed using the techniques illustrated in the paper.

AMTD
6, 6147–6186, 2013

1 Introduction

Organic compounds comprise an important subset of atmospheric constituents and can exist in all atmospheric phases, i.e. gas, particle and aqueous. It is known that organics play important roles in determining the abundance of atmospheric oxidants and influencing the properties of suspended particles and aqueous droplets, affecting climate and human health (Hallquist et al., 2009; Ervens et al., 2011). Global-scale measurements of aerosol particles have assigned 20–90 % of sub-micron aerosol mass to be organic (Zhang et al., 2007; Jimenez et al., 2009), with much of this material secondary in nature (i.e. Secondary Organic Aerosol or SOA) having been formed in the atmosphere through the condensation of oxidation products of volatile precursors or from in-cloud oxidation processes (Kanakidou et al., 2005; Hallquist et al., 2009; De Gouw and Jimenez, 2009; Ervens et al., 2011). There are thought to be hundreds to thousands of organic compounds within SOA, which may undergo chemical processing in the atmosphere after condensation (Hamilton et al., 2004).

While gas phase oxidation reactions have been studied extensively, there is a growing demand on advanced analytical techniques which allow for the detection and elucidation of condensed phase organic species and to assist in understanding their transformations, sources and sinks (Duarte and Duarte, 2011; Laskin et al., 2012; Pratt and Prather, 2012a, b). Such techniques can vary in sensitivity, specificity, and time response. The ability of such techniques to be deployed in the field is highly desirable because a comprehensive understanding of organic processing requires both lab and complementary field measurements.

A wide range of spectroscopic techniques has been utilized to successfully investigate the organic composition of particulate matter (PM) and cloud-, fog- and rain-water, including Nuclear Magnetic Resonance (NMR) (Decesari et al., 2000, 2007, 2011; Duarte et al., 2007; Cleveland et al., 2012; Finessi et al., 2012; Santos et al., 2012; Shakya et al., 2012), Fourier Transform Infrared (FT-IR) (Sax et al., 2005; Duarte et al., 2007; Polidori et al., 2008; Takahama et al., 2013) and Ultraviolet–visible (UV-Vis) spec-

AMTD
6, 6147–6186, 2013

troscopy (Decesari et al., 2000; Duarte et al., 2005; Walser et al., 2007; Moosmueller et al., 2009; Wagner et al., 2009; Shapiro et al., 2009; Bones et al., 2010; Santos et al., 2012; Gyawali et al., 2012). All such spectroscopic measurements provide information on organic aerosol bulk properties with specificity restricted to individual functional groups. For example, proton NMR (^{1}H-NMR) directly provides quantitative information on the amount of aldehydic, hydroxyl and aromatic groups, whereas, ketone and carboxylic acid functionalities can be measured indirectly (Decesari et al., 2007) or via derivatization (Moretti et al., 2008). FT-IR gives more direct quantitative information on the carbonyl functional groups and has been implemented in PM and cloud studies (Sax et al., 2005; Duarte et al., 2007; Polidori et al., 2008; Wagner et al., 2009; Russell et al., 2009; Takahama et al., 2013). However, FT-IR can be prone to inorganic interferences, which are likely present in atmospheric samples (Duarte et al., 2007; Polidori et al., 2008). In addition, better resolution of individual constituents requires chromatographic separation prior to analysis (Polidori et al., 2008). UV-Vis has been used for brown carbon (BrC) measurements (Moosmueller et al., 2009; Wagner et al., 2009). However, the fact that only multi-conjugated functional groups are detected implies the need for complementary analytical techniques to characterize the whole organic composition. A common limitation of these spectroscopic techniques is the requirement of a large amount of sample due to low sensitivity, which subsequently results in low time resolution (Duarte and Duarte, 2011).

As a complement to spectroscopic techniques, mass spectrometry is increasingly being applied for measurement of condensed phase atmospheric organics because it has the potential to provide quantitative chemical formula information with very high sensitivity. Approaches vary via their means of vaporizing the constituents, in their ionization methods and in the mass analyzers employed. Widely used instruments are the Aerodyne Aerosol Mass Spectrometer (AMS), which is based on Electron Ionization (EI) with flash vaporization at 600 degrees, and single-particle approaches that use lasers for both particle vaporization and/or ionization (Murphy and Thomson, 1995; Gard et al., 1997; Canagaratna et al., 2007; Onasch et al., 2012). AMS instruments

AMTD
6, 6147–6186, 2013

are field deployable and have emerged as a very powerful tool to study PM (Canagaratna et al., 2007; Zhang et al., 2007; Jimenez et al., 2009) and more recently fog and cloud droplets (Ge et al., 2012; Lee et al., 2012). The attraction of the AMS is the ability to derive quantitative information of inorganic and organic constituents in an on-line manner (Canagaratna et al., 2007). While measurements from the AMS have substantially improved the understanding of PM evolution in the atmosphere, much molecular information is lost due to significant fragmentation during the hard ionization by EI (Canagaratna et al., 2007).

Electro-Spray Ionization (ESI) Mass Spectrometry (ESI-MS) has been used in several lab and field studies to elucidate the organic aerosol and fog water composition (Altieri et al., 2008; Perri et al., 2009; Tan et al., 2009, 2010; Schmitt-Kopplin et al., 2010; Lim et al., 2010; Mazzoleni et al., 2010; Kundu et al., 2012). The advantage of ESI-MS is the soft ionization of ESI, in which the analyte ion stays intact; as well, the sample is not heated before ionization. Also, ESI-MS instruments are sometimes equipped with high resolution Fourier transform ion cyclotron mass spectrometer (FTICR-MS) and other high resolution instruments, by which molecular level information for individual species can be drawn from very complex samples (Laskin et al., 2012, 2013). The application of ESI-MS in aerosol research has substantially improved the understanding of aerosol evolution and processing in the atmosphere (Perri et al., 2009; Tan et al., 2009, 2010; Laskin et al., 2012, 2013). However, in this technique the sample must be mixed with a solvent that is required to induce ionization, which might lead to unwanted bulk reactions between the analyte and the solvent (Bateman et al., 2008). Most importantly, ESI-(FTICR)-MS instruments are not yet field deployable for on-line measurements.

While the technique of Chemical Ionization Mass Spectrometry (CIMS) has been used in atmospheric chemistry to make gas phase measurements for decades, it has only now been applied to the study of organic processing that takes place in atmospheric cloud-,fog- and rain-water, and particles (Thornton et al., 2003; Hearn and Smith, 2004; Thornton and Abbatt, 2005; Sareen et al., 2010; Ervens et al., 2011; Zhao

AMTD
6, 6147–6186, 2013

et al., 2012). An advantage of the CIMS over other mass spectrometry techniques is the ability to use a variety of reagent ions that induce the chemical ionization in order to selectively detect certain classes of organic compounds of interest. Most importantly, chemical ionization is a relatively soft ionization technique and thus the analyte ion is often not fragmented. This is important if information at the molecular level is desired, such as in mechanistic and kinetic studies. However, as the sample composition becomes more complex, the low resolution quadrupole mass analyzer used previously with CIMS instruments becomes inadequate to resolve the whole organic composition (Hearn and Smith, 2006), and higher resolution instruments are preferred.

Aerosol studies utilizing the CIMS rely on thermal desorption to volatilize the organic constituents of the particles, since these organics are of low volatility. For instance, a multi-orifice volatilization impactor (MOVI) has recently been developed as an interface to CIMS instruments, which allows for on-line separation of gas and particle phase organics (Yatavelli and Thornton, 2010; Yatavelli et al., 2012). While particles are collected on the MOVI, gaseous species are detected by the CIMS. After particle collection ends, the impactor is heated gradually and organics volatilize off depending on their vapour pressures. Thus, it can also provide vapour pressure information of the species being analyzed. Another interface that has been previously employed in aerosol studies is the aerosol-CIMS (or thermal desorption CIMS, TD-CIMS) (Hearn and Smith, 2004, 2006; Sareen et al., 2010; Zhao et al., 2012). The aerosol-CIMS can detect both gas and particle phase constituents simultaneously on-line by introducing a heated inlet to volatilize particle phase components.

This paper illustrates the potential of high resolution time-of-flight aerosol-CIMS (CI-ToFMS) to study the composition of a complex organic matrix in the atmosphere, namely the water soluble organic compounds (WSOC) of α-pinene ozonolysis SOA. We treat this complex organic mixture and its subsequent aqueous photo-oxidation components as models to highlight the capabilities of high resolution aerosol-CI-ToFMS to study organic aerosol composition and processing. We illustrate how a comprehensive analysis can be achieved by choosing the CI-ToFMS reagent ions to selectively

AMTD
6, 6147–6186, 2013

ionize certain classes of organic compounds within the WSOC SOA. In particular, three reagent ions: (1) protonated water clusters $(H_2O)_nH^+$, (2) acetate anions, $CH_3C(O)O^-$ and (3) iodide water cluster $I(H_2O)_n^-$ ions were used to explore their selectivity for the same change in chemical composition occurring during WSOC photo-oxidation. The results are presented as oxygen-to-carbon atomic ratios (O/C), hydrogen-to-carbon atomic ratios (H/C), carbon oxidation state (OS_C) and numbers of carbon atoms (#C) distributions over the course of aqueous phase oxidation for the three reagent ions. For reference, we compare the data to those simultaneously obtained with high resolution AMS. Furthermore, we illustrate that different chemical classes, corresponding to monomers and dimers of the α-pinene oxidation products, were observed for the WSOC in all the three reagent ions CI-ToFMS spectra. The differing rates of oxidation of the monomer and dimer species illustrate how aerosol-CI-ToFMS can be utilized to study chemical change within a chemically complex matrix. The detailed mechanistic interpretation of the oxidative evolution of the hundreds of peaks within the aerosol-CI-ToFMS spectra, along with selected kinetics studies of major constituents, will be presented in a subsequent publication.

2 Experimental

The experiments were carried out in the following sequence: (1) SOA generation and collection, (2) aqueous phase photo-oxidation of WSOC and (3) detection of photo-oxidation products using high resolution CI-ToFMS and AMS (Aerodyne Inc.).

2.1 SOA generation and collection

The reaction of ozone with α-pinene was used to generate SOA in a continuous manner in the University of Toronto Mobile Oxidation, Concentration and Aging (MOCA) chamber (i.e. FEP Teflon bag, 1 m^3 volume). An OH radical scavenger was not added and as a result α-pinene was oxidized by both ozone and OH, and no seed aerosol

AMTD
6, 6147–6186, 2013

was employed. The experimental setup is illustrated in Fig. 1. The chamber was run in the dark at room temperature and pressure. Dry (RH ~ <5 %), purified, hydrocarbon free air, from a pure air generator (Model 737, AADCO), was the carrier gas and flowed continuously into the chamber before the reagents were introduced. All flows were controlled using mass flow controllers (MKS). Ozone was generated by passing 0.1 LPM (Liter per minute) of purified air over a mercury lamp. α-Pinene (Aldrich, >99 %) was injected continuously in 1 LPM of air using a 25 µL syringe (Hamilton) mounted on a syringe pump (Harvard Apparatus, Pump11 Elite) at a rate of 0.1 µL min^{-1}. In order to reduce the concentration of α-pinene in the chamber, 0.1 LPM of the air carrying α-pinene was introduced in the chamber while the rest flowed to the exhaust. A needle valve was placed on the exhaust line to insure sufficient pressure is present to allow 0.1 LPM α-pinene flow into the chamber (see Fig. 1). Makeup air of 10.5 LPM was added in order to dilute the reagents and to give a residence time of ~ 1.6 h in the chamber. A pump was connected to the chamber outlet to pull 8.9 LPM of air through an O_3 denuder to remove part of the ozone.

An ozone analyzer (model 49i, Thermo scientific) was used to monitor the O_3 concentration in the chamber, α-pinene concentration was monitored with a Proton Transfer Reaction-Mass Spectrometry (PTR-MS, Ionicon) by following m/z 137 and 81, and the SOA size distribution was measured using a TSI Scanning Mobility Particle Sizer (SMPS, 3081 Differential Mobility Analyzer (DMA), 3025A Condensation Particle Counter (CPC)). Typical time profiles for the reagents and SOA mass loading (assuming a density of 1.2 g mL^{-1}) are shown in Fig. 2. When the reagents and SOA loading reached a stable level (Fig. 2), a Teflon filter (47 mm diameter and 2 µm pore size, Pall life sciences) was placed downstream of the ozone denuder (Fig. 1). SOA was collected on the filter for 6–8 h and the aerosol mass collected (0.5–0.7 mg per filter) was determined by an electronic balance before and after SOA collection. Immediately after SOA was collected, the filter was immersed in ~ 50 mL of purified water (18 mΩ cm, Veolia) in a plastic bottle (Nalgene), which was pre-rinsed with purified water. The immersed filter was shaken for ~ 15 min and then left in the freezer at −30 °C.

AMTD
6, 6147–6186, 2013

2.2 Aqueous phase photo-oxidation of WSOC

The aqueous phase photo-oxidation reaction was carried out in a photo-reactor (Rayonet Reactor, RPR-200) equipped with UV-B lamps (RPR-3000, peak emission at 310 nm) mounted in a circular manner such that they are equidistant from the centre. A stirring plate and a fan were added to the photo-reactor to ensure adequate solution mixing and cooling, respectively. The aqueous solutions were placed in a glass bottle (Wheaton) in the centre of the photo-reactor, and thus light of wavelengths greater than 300 nm was transmitted to the sample. The solution temperature when the lamps were on was 28 °C. Hydrogen peroxide (Sigma-Aldrich, ≥ 30 % in water, TraceSELECT) was added to the sample such that a 1 mM concentration is present. The aqueous phase OH photo-oxidation was initiated by the photolysis of hydrogen peroxide to form OH. From the decay of species with known rate constants with OH (i.e., cis-pinonic acid), we estimate that the steady state OH concentration is on the order of $(1.1 \pm 0.1) \times 10^{-13}$ M.

Three frozen WSOC solutions were allowed to thaw at room temperature and combined. Purified water (18 mΩ cm, Veolia) was added to make a 200 mL solution of $\sim 10\,\mu g\,mL^{-1}$ SOA mass in water. The 200 mL solution was divided into 4 × 50 mL aliquots. 1 × 50 mL aliquot was used to carry out the OH oxidation and 2 × 50 mL solutions were used for photolysis (i.e. no H_2O_2) and dark (i.e. H_2O_2 but no light) control experiments, and 1 × 50 mL was a backup. A volume of 5.13 µL of hydrogen peroxide was injected in the SOA solution to give a concentration of 1 mM. The oxidation was initiated by the irradiation of UV-B lamps. The photo-oxidation and control experiments were allowed to run for 4 h, where the photo-oxidized sample was exposed to a total of 1.6×10^{-9} M s of OH.

2.3 Detection of WSOC and the photo-oxidation products

The WSOC solution was atomized using a TSI constant output atomizer (model 3076). A fraction of the droplets was diluted by a factor of 4 with nitrogen gas (BOC, grade 4.8) or air (Linde, grade 0.1) before entering the HR-CI-ToFMS (Aerodyne Inc.) (Fig. 3).

AMTD
6, 6147–6186, 2013

In order to volatilize the organics from the droplets, the diluted flow was heated up to 150 °C by passing it through a 70 cm long Siltek-coated stainless steel tubing (Restek). The tubing was heated by wrapping it with a heating tape (Omega, STH051) and the temperature was controlled using a modified temperature controller (Omega, CN1A-TC). The residence time in the heated line was about 1.4 s. Temperature ramping experiments were carried out where the temperature of the line was ramped from 100 °C to 250 °C in steps of 50 °C. The line temperature (of 150 °C) was selected such that the signal for the majority of the ions of interest was maximized. These observations were consistent with Yatavelli et al. (2012), where the thermogram of α-pinene ozonolysis particle phase showed that the product of m/z 155–357 peaked in signal at temperatures below 150 °C. Approximately 0.8 LPM of the unheated droplet flow was diluted by air (Linde, grade 0.1) (see Fig. 3) and passed through a diffusion dryer. The flow was then introduced to the HR-AMS (Aerodyne Inc.) and the SMPS (TSI, 3081 DMA, 3776 CPC). A pump was also connected to the manifold downstream of the dryer in order to reduce the residence time of the droplets in the tubing downstream from the atomizer.

2.3.1 HR-CI-ToFMS

A detailed description of the HR-CI-ToFMS can be found in Bertram et al. (2011) and Yatavelli et al. (2012). The sample flow rate entering the low pressure ion-molecule reaction (IMR) chamber of the CI-ToFMS was set to 2.0 LPM by a critical orifice.

The reagent ions used in this work were: protonated water cluster $(H_2O)_nH^+$, acetate anions $CH_3C(O)O^-$ and iodide water clusters $I(H_2O)_n^-$. A fritted glass bubbler was used to bubble water (18 mΩ cm) with 2.2 LPM of nitrogen to generate water vapor for creating $(H_2O)_nH^+$. Acetate reagent ions were generated by a flow of 10 sccm from the acetic anhydride (Sigma, 539996) headspace contained in a stainless steel bottle (Swagelok) in room temperature, which was subsequently diluted by 2.2 LPM of nitrogen. A home-built permeation tube left at room temperature containing methyl iodide (Sigma, I8507) was the source required to create the iodide water cluster reagent ions. Each reagent ion precursor passed through a ^{210}Po radioactive cell (NRD, Model

AMTD
6, 6147–6186, 2013

2031), at a flow of 2 LPM set by a critical orifice, in order to create the ionization reagent ions. The analyte ionization took place by the following chemical ionization reactions:

$$\text{Protonated water clusters}: (H_2O)_nH^+ + M \longrightarrow n(H_2O) + MH^+ \quad \text{(R1)}$$

$$\text{Acetate}: CH_3C(O)O^- + MH \longrightarrow CH_3C(O)OH + M^- \quad \text{(R2)}$$

$$\text{Iodide water clusters}: I(H_2O)_n^- + M \longrightarrow n(H_2O) + I(M)^- \quad \text{(R3)}$$

The IMR pressure and temperature were adjusted to 96 ± 1 mbar and 57 °C, respectively. The pressure of the collisional dissociation chamber (CDC), the chamber following the IMR containing the short segmented quadrupoles (SSQ), was controlled to 2.0 ± 0.2 mbar. A nitrogen flow was used to dilute the sample flow in the $(H_2O)_nH^+$ and $I(H_2O)_n^-$ reagent ion experiments (Fig. 3), while a flow of air was used for the dilution in the $CH_3C(O)O^-$ reagent ion experiments. This was essential as the acetate reagent ion concentration seemed to be sensitive to the amount of oxygen present.

The fields' strength within the CI-ToFMS controls the amount of gas phase ion clustering and fragmentation. Protonated water clusters and iodide water clusters reagent ions experiments were run in weak-field mode. This is because fragmentation was observed for the sample ions in the $(H_2O)_nH^+$ experiments when moderate- to strong-fields were applied. Also, in the $I(H_2O)_n^-$ case, the analyte ion is detected clustering with I^- as illustrated in Reaction (R3) and the weak field insures that the cluster stays intact to maximize the overall signal. In contrast, acetate reagent ion experiments were run in strong-field mode, because a mixture of deprotonated analyte (Reaction R2) and analyte clustering with acetate ions were observed in weak-field mode. To minimize complexity of ion assignment, a strong-field insured that the majority of the peaks in the mass spectra followed Reaction (R2). A list of the voltages in the mass spectrometer used to run the experiments is given in Table S1. All experiments were run in

AMTD
6, 6147–6186, 2013

V-mode with the time-of-flight mass spectrometer, and data were acquired at 1 s time resolution and averaged to 5 min using the data analysis software, Tofware 2.2.2 (Aerodyne Inc.). Peak fitting and ion assignment were performed for all peaks in the spectra for the three reagent ion up to molecular weight of 300 u. The mass accuracy for all V-mode experiments was ±5 μTh Th^{-1} (ppm). The ToF resolving power was 4285 (at m/z 301), 4194 (at m/z 299) and 4186 (at m/z 427) for $(H_2O)_nH^+$, $CH_3C(O)O^-$ and $I(H_2O)_n^-$, respectively. More details regarding mass accuracy and resolving power of the mass spectrometer can be found elsewhere (Bertram et al., 2011; Yatavelli et al., 2012; Jokinen et al., 2012). Data for the three reagent ions were normalized to reagent ion signal and background subtracted.

2.3.2 HR-AMS

The aqueous particles passed through a diffusion dryer and were subsequently analyzed by the HR-AMS for determination of non-refractory components. The working principle of the AMS has been reviewed by (Canagaratna et al., 2007). The HR-AMS switched between V-mode (1 min) and W-mode (4 min) during the experiments. The data analysis was performed using Squirrel (version 1.51H) and Pika (version 1.10H). The standard fragmentation table in Pika with the corrected air fragment column for our carrier gas were used. The elemental analysis of W-mode data was performed with the default correction factors for O/C (0.75) and H/C (0.91) in Pika (Aiken et al., 2008).

2.4 Sensitivity evaluation

To evaluate relative sensitivities of different species, the following organic compounds were used: glyoxal (Sigma, 40 wt. % in H_2O), methylglyoxal (Sigma, 40 % in H_2O), formic acid (Sigma, 50 wt. % in H_2O), acetic acid (Fisher, 99.9 %), glyoxylic acid (Sigma, 50 wt. % in H_2O), pyruvic acid (Sigma, 98 %), pinonic acid (Sigma, 98 %), oxalic acid (Fisher, 99.9 %), malonic acid (Sigma, 99 %), succinic acid (Fisher, 99.7 %), levoglucosan (Sigma, 99 %), citric acid (Sigma, ≥ 99.5 %) and L-tartaric acid (Fisher,

AMTD
6, 6147–6186, 2013

> 99.5 %). Three standard solutions of a combination of the thirteen organic compounds were prepared in purified water (18 mΩ cm). The concentrations of each of the organic compounds were 5, 15 and 25 µM. The standard solutions were sampled as illustrated in Fig. 3, with the CI-ToFMS operating with the three reagent ions separately. The sensitivity of each compound was obtained from the slope of the three-point calibration curve.

3 Results and discussion

3.1 CI-ToFMS sensitivity and Selectivity evaluation

The sensitivity of 13 organic compounds with known concentrations in the aqueous phase was assessed using the CI-ToFMS with the three reagent ions. This test was performed in order to evaluate the selectivity of each reagent ion towards known organic compounds. The organic compounds were chosen such that a variety of functional groups are presented.

Figure 5a shows the sensitivities of the 13 compounds using $(H_2O)_nH^+$ reagent ions. The sensitivities obtained for all compounds are relatively low with the exception of cis-pinonic acid and succinic acid. The proton transfer reaction (R1) is governed by the gas phase affinity of the organic compounds to protonate. The reaction proceeds if the gas phase basicity of the analyte is higher than that of the water clusters, $(H_2O)_n$. The reagent cluster ions observed in the spectra were with n = 3, 2, 4 listed by descending intensity, although this may not reflect the nature of the cluster distribution in the IMR and it is unknown which combination of the water cluster ions ionizes the analyte. The gas phase basicity of the clusters are 730, 694 and 769 kJ mol^{-1}, respectively (NIST, 2013). Gas phase basicity data are not available for the majority of the organic compounds, except for formic acid (710 kJ mol^{-1}) and acetic acid (753 kJ mol^{-1}) (Hunter and Lias, 1998). The gas phase basicity of acetic acid is higher than n = 2 and 3 water clusters. However, formic acid gas phase basicity is only higher than that of the n = 2

AMTD
6, 6147–6186, 2013

water cluster. Formic acid was not observed in the $(H_2O)_nH^+$ reagent ion spectra at all concentrations, unlike acetic acid. This indicates that the proton transfer reaction from $(H_2O)_nH^+$ to formic acid did not proceed. In addition, according to these observations, $(H_2O)_nH^+$ clusters with $n \geq 3$ appear to be playing a role in the proton transfer reaction. This also suggests the possibility that the actual distribution of $(H_2O)_nH^+$ clusters is with $n \geq 3$ in the IMR. The observation of $n = 2$ cluster in the mass spectra was probably due to fragmentation of higher order clusters yielding $n = 2$ cluster. However, this interpretation is based on the data from only two organic compounds and more information regarding other compounds is required before a conclusive understanding can be drawn. It appears from Fig. 5a that all the multi-functional organic compounds have relatively low sensitivities compared to pinonic acid, malonic acid, succinic acid, levoglucosan and citric acid, all of which contain reduced carbons ($-CH_2-$). This illustrates the selectivity of $(H_2O)_nH^+$ reagent ions toward compounds that are not highly oxygenated.

Details about the $CH_3C(O)O^-$ ionization method can be found elsewhere (Veres et al., 2008). Ionization takes place if the gas phase acidity of the analyte is higher than that of acetic acid. It has been found that acetic acid has a low gas phase acidity and thus most acids can deprotonate via Reaction (R2) (Veres et al., 2008). The sensitivity of the CI-ToFMS to the organic compounds using acetate reagent ions is shown in Fig. 5b. All acids were detected in the deprotonated form and all the non-acid bearing compounds were not detected sensitively, with the exception of levoglucosan, which was detected as a cluster with $CH_3C(O)O^-$. Interestingly, the majority of the acids have more uniform sensitivities, with less than a factor of 4 difference, when compared to Fig. 5a and c. In addition, small compounds such as formic, glyoxylic and pyruvic acids ($C < 3$) and large organic acid compounds show similar sensitivities. The results demonstrate that $CH_3C(O)O^-$ reagent ions are selective to acids in general, in accord with the work of (Veres et al., 2008). However, compounds with non-acid functionality (e.g., levoglucosan) can also be observed clustering with $CH_3C(O)O^-$.

AMTD
6, 6147–6186, 2013

$I(H_2O)_n^-$ reagent ions data are shown in Fig. 5c. The ionization by Reaction (R3) has been described earlier (Caldwell and Kebarle, 1984) and used extensively in atmospheric studies (Thornton and Abbatt, 2005; Zhao et al., 2012). The ionization depends on the ability of the organic compounds to hydrogen bond with the iodide anion. In addition, since iodide is a large polarisable anion, compounds with large polarisability, such as those with high molecular weight and those containing double bonds, will be better detected. As can be seen in Fig. 5c, multi-functional compounds with $C > 3$ can be detected with very similar sensitivities. Those compounds are di-acids, tri-acids and alcohols, all of which can participate in hydrogen bonding with the iodide and at the same time are more polarisable by size. Glyoxylic acid, which has aldehydic and acidic groups, was also detected with a good sensitivity similar to the multi-acids and unlike its analogues, pyruvic acid. This is possibly due to the fact that aldehydic hydrogen in glyoxylic acid is slightly electron deficient and thus can form a hydrogen bond with the iodide in contrast to the methyl group hydrogens in pyruvic acid. The aldehydes, glyoxal and methylglyoxal, were not detected well. These two aldehdyes have been previously detected in the hydrated gas phase forms after volatilization from a solution using $I(H_2O)_n$ reagent ions (Zhao et al., 2012). However, these previous measurements using aerosol-CIMS were carried out at lower heated inlet temperatures (110 °C). Thus, it is possible that dehydration of the aldehydes was more efficient at 150 °C, which was the temperature used in this study. As a result, the ability of binding to iodide was reduced.

Overall, $I(H_2O)_n^-$ and $CH_3C(O)O^-$ were found to be best in detecting multifunctional organic compounds which could particularly be useful for detecting oxygenated organic aerosol (OOA) components that are generally observed in the field.

3.2 WSOC and Aqueous photo-oxidation processing

Four hour aqueous photo-oxidation experiments of the WSOC were followed using the CI-ToFMS using the three reagent ions. In all cases the control experiments (not shown) conducted with either H_2O_2 present but not light, or vice versa, showed negligi-

AMTD
6, 6147–6186, 2013

ble chemical change as compared to the photo-oxdiation results arising from when both are present. As a result, only data from photo-oxidation experiments are presented.

3.2.1 Raw mass spectra

Mass spectra were collected every second for 4 h of oxidation. The mass spectra obtained for the WSOC before oxidation and after 2 and 4 h of oxidation are shown in Fig. 6. As the reaction proceeds, regions where ions decay are shown in the left spectra and regions where ions form are shown in the right spectra. All spectra before the oxidation was initiated show two humps, monomers and dimers regions, where the monomer region corresponds to ions with molecular weight similar to cis-pinonic and cis-pinic acids i.e. primary oxidation products of a-pinene. Dimeric species are thought to arise via (1) ester, acetal and peroxy-acetal formation in the aqueous phase, (2) gas phase oxidation in the chamber before the SOA was collected or (3) droplet evaporation in the heated inlet. It is clear that the dimer region in the three reagent ions spectra is decaying during photo-oxidation. In addition, the majority of the products formed after 2 and 4 h of oxidation lie in a lower molecular weight monomer region. This is one indication that fragmentation (and functionalization) reactions are possibly occurring within the organic species during oxidation. By comparing the time dependent spectra of the dimer to monomer region in the $I(H_2O)_n$ spectra, it is clear that the dimers decay at a much faster rate compared to the monomers. This could be due to the fact that dimer reactions lead to monomers (fragmentation), which subsequently appear as if the monomers are slowly reacting.

The observation that the $I(H_2O)_n$ spectra are showing the largest and most clear decay compared to $CH_3C(O)O^-$ and $(H_2O)_nH^+$ spectra may be due to gas phase ion cluster formation for the two latter reagent ions. To illustrate, it was observed (not shown) in the sensitivity test (Sect. 3.1) the presence of ions for $(H_2O)_nH^+$ and in $CH_3C(O)O^-$ reagent ions, which was not expected based on Reactions (R1) and (R2). These ions form by gas phase clustering between ions formed in Reactions (R1) and (R2) with non-ionized analyte compounds, and thus show up as high molecular weight ions.

AMTD
6, 6147–6186, 2013

These gas phase ion clusters can be a combination of (1) an analyte ion and another analyte or (2) an analyte ion and a reagent ion related species such as H_2O clusters or acetic acid/acetic anhydride. Such ions did not show up in the $I(H_2O)_n$ spectra. As a result, the dimer region in $(H_2O)_nH^+$ and in $CH_3C(O)O^-$ contains a combination of real dimers existing in aqueous solution (or formed during the droplet evaporation process), such as those that appear in the $I(H_2O)_n$ spectra, and those formed by gas phase ion clusters.

3.2.2 Ion Assignment and Speciation

Peak fitting was performed for all three reagent ion spectra covering chemical formulas with molecular weights up to 300 u (m/z 301, m/z 299 and m/z 427 for $(H_2O)_nH^+$, $CH_3C(O)O^-$ and $I(H_2O)_n^-$, respectively). Peaks higher than 300 u cannot be unambiguously assigned for the $(H_2O)_nH^+$, $CH_3C(O)O^-$ reagent ions. Chemical formulas were assigned for odd m/z based on selection criteria governed by the following chemical formula $C_nH_{2n+2}O_x$, where formulas assigned cannot have a number of hydrogen atoms greater than $2n+2$ for a given carbon number equal to n. Elements other than C, H and O were not considered in the formula predictions as it was assumed that those elements were absent from the reagents (WSOC and H_2O_2) and purified water. The peaks were fit with the minimum number of ions such that a residual area (un-fitted area) of less than 5 % is achieved. Isotopic patterns were used to confirm ion assignments in some cases. The number of ions assigned were 595, 555 and 428 for $(H_2O)_nH^+$, $CH_3C(O)O^-$ and $I(H_2O)_n^-$, respectively. The smaller number of ions assigned for the same chemical composition with $I(H_2O)_n^-$ compared to the other reagent ions is an indication of the selectivity of $I(H_2O)_n^-$.

From the ion lists generated for the spectra, hydrogen-to-carbon ratios (H/C), oxygen-to-carbon ratios (O/C) and the number of carbon atoms (#C) were derived for the individual chemical formulas. The carbon oxidation state (OS_C) was calculated as described in (Kroll et al., 2011) by the approximation $OS_C \approx 2\,O/C + H/C$. The ion chemical formulas were corrected for the proton added when using $(H_2O)_nH^+$, and

AMTD
6, 6147–6186, 2013

subtracted in the case of $CH_3C(O)O^-$, such that the neutral chemical formula of the analytes was used for calculations and plotting. Also, gas phase ion clusters cannot be separated from non-cluster ions that appear at the same m/z as both could have the same chemical formula. The distribution of the 4 parameters H/C, O/C, OS_C and #C for the ions lists is shown in Fig. 7 as percentile box plots.

The ions assigned in the $(H_2O)_nH^+$ spectra cover noticeably narrower H/C, O/C and OS_C ranges as compared to $CH_3C(O)O^-$ and $I(H_2O)_n^-$. In addition, the H/C distribution spans a higher H/C region ranging from 1 to 2 compared to 0.6–2 for the other reagent ions. Lower O/C and OS_C values for all the percentiles are also observed for $(H_2O)_nH^+$. The $CH_3C(O)O^-$ and $I(H_2O)_n^-$ percentiles for the 4 parameters are very similar overall. This indicates that the assigned ions in the two reagent ions spectra are similar, although with some selectivity associated with $I(H_2O)_n^-$. These results are consistent with the observation in Sect. 3.1, where highly oxygenated multi-functional organics were detected with high sensitivity with $CH_3C(O)O^-$ and $I(H_2O)_n^-$ but not with $(H_2O)_nH^+$. It is noted also that these two reagent ions ($CH_3C(O)O^-$ and $I(H_2O)_n^-$) can detect some species with extremely high OS_C, approaching 3.7 and 4, and O/C, approaching 2.75 and 3, respectively.

3.2.3 The Van Krevelen diagram

The intensity of each ion together with the H/C and O/C values were used to calculate the intensity weighted average elemental ratios, $\overline{H/C}$ and $\overline{O/C}$. This allows plotting the time dependent $\overline{H/C}$ and $\overline{O/C}$ for the photo-oxidation reaction in a Van Krevelen diagram (Heald et al., 2010; Ng et al., 2011). One question of interest is the degree to which Van Krevelen diagram is similar to data that are derived from the AMS instrument. Figure 8b expands the Van Krevelen diagram to emphasize the differences between the data for the CI-ToFMS three reagent ions and the AMS. As a reference point, it is interesting that the slope of the linear fit of the AMS data is −0.48, which is essentially the same as the slope of −0.5 found by Ng et al. (2011) from a compilation

AMTD
6, 6147–6186, 2013

of aerosol ambient and chamber SOA data affected by aging. As well, Fig. 8a illustrates that the CI-ToFMS and AMS data largely overlap in the H/C and O/C spaces, with the CI-ToFMS data lying within the accuracy range of the AMS data. This close agreement is somewhat surprising given the use of uncalibrated CI-ToFMS ion intensity, which is not necessarily a good approximation to the true analyte abundances. As well, the AMS detects only particle phase organics, while the aerosol-CI-ToFMS detects both gas and particles phase components.

Figure 8b highlights the differences between the three CI-ToFMS reagent ions. The data show that the maximum $\overline{O/C}$ obtained with $(H_2O)_nH^+$ was 0.53, while $CH_3C(O)O^-$ and $I(H_2O)_n^-$ maxima were 0.75 and 0.71. This illustrates the inability of $(H_2O)_nH^+$ reagent ions to efficiently ionize highly oxygenated organics, especially those present at the end of the oxidation reaction. Correspondingly, the trajectory of the $(H_2O)_nH^+$ $\overline{O/C}$ and $\overline{H/C}$ data series always lags in time behind those for $CH_3C(O)O^-$ and $I(H_2O)_n^-$. While $CH_3C(O)O^-$ and $I(H_2O)_n^-$ follow a similar path in $\overline{O/C}$ as the reaction proceeds, their $\overline{H/C}$ values slightly diverge at $\overline{O/C}$ of 0.6, where the $I(H_2O)_n^-$ data stay closer to the AMS data. As discussed in Sect. 3.1 (i.e., sensitivity evaluation), $CH_3C(O)O^-$ reagent ions allow for efficient detection of carboxylic acids in general and show no discrimination in ionizing small acids, which are relatively volatile (or semi-volatile) and are not detected by the AMS. Thus, more volatile species with higher H/C may be detected by $CH_3C(O)O^-$ causing a divergence from the AMS data. For instance, Fig. 5b shows that $CH_3C(O)O^-$ allows detecting formic acid (H/C = 2) in similar sensitivity as other multifunctional acids such as citric acid (H/C = 1.3). On the other hand, Fig. 5c illustrates that formic acid sensitivity is approximately an order of magnitude less than that of citric acid with $I(H_2O)_n^-$ reagent ions. Formic acid is relatively volatile and is not detected by the AMS unlike citric acid, which can form particles detected by the AMS. Thus, the signal of formic acid is masked in the $\overline{H/C}$ calculation for the $I(H_2O)_n^-$ case making the $\overline{H/C}$ and $\overline{O/C}$ trajectories similar to those from the AMS. Thus, it

AMTD
6, 6147–6186, 2013

is reasonable that the $I(H_2O)_n^-$ data converge to those from the AMS, given that the CI-ToFMS data are likely dominated by particle-phase species (i.e., less volatile, large acids and multifunctional organics).

3.2.4 The Difference Kroll Diagram

The 2-D space of the other two parameters OS_C and #C, the so-called Kroll diagram, can also be used to obtain more informative evidence on the nature of chemical change (Kroll et al., 2011). In a typical Kroll diagram, the OS_C is plotted as a function of #C. Here, the CI-ToFMS is advantageous over the AMS as it provides carbon number information directly for individual ions. This feature of CI-ToFMS arises from the soft ionization ability that frequently retains the ions intact without fragmentation. In addition, the CI-ToFMS provides a means by which bulk or individual compound OS_C and #C values can be obtained. The $\overline{OS_C}$ and $\overline{\#C}$ are the intensity weighted averages of OS_C and #C summed over all individual ions.

In order to observe a change in the OS_C and #C distribution for individual compounds over the 4 h of photo-oxidation, a difference-Kroll diagram was constructed as shown in Fig. 9. In the difference-Kroll diagram the intensities of ions with the same co-ordinates on the plot are summed at time 0 and 4 h. The Kroll diagram information at time 4 h is subtracted from that at time 0. Coordinates with positive intensity are those that decay away and are marked in light coloured solid circles. Negative intensities indicate coordinates where ions have formed after 4 h of photo-oxidation and are marked in solid dark coloured circles. The highest OS_C in the difference Kroll diagram for $(H_2O)_nH^+$ is 1.33. On the other hand, the plots for $CH_3C(O)O^-$ and $I(H_2O)_n^-$ clearly show many occupied coordinates with OS_C ranging from 2 to 4, i.e. very highly oxidized species, with #C less than 10. All three reagent ion difference Kroll diagrams show that the majority of the ions formed after 4 h of oxidation have a lower carbon number and higher oxidation state compared to the original state, consistent with a large degree of functionalization and fragmentation occurring in the reaction (Kroll et al., 2009). In addition, the verti-

AMTD
6, 6147–6186, 2013

cal distribution (OS_C) of the ions in the $I(H_2O)_n^-$ Kroll diagram is narrower compared $CH_3C(O)O^-$, which is consistent with the selectivity observed for $I(H_2O)_n^-$ in Sect. 3.1.

The $\overline{OS_C}$ and $\overline{\#C}$ reflect how the whole distribution is moving over 4 h of oxidation. The change in $\overline{OS_C}$ and $\overline{\#C}$ is most obvious with $CH_3C(O)O^-$ and $I(H_2O)_n^-$ reagent ions while a small change is observed in the $(H_2O)_nH^+$ Kroll diagram, in large part because this latter reagent ion is insensitive to many of the more highly oxidized species that are forming. In all three cases, the $\overline{OS_C}$ and $\overline{\#C}$ trajectory indicates that both fragmentation and functionalization reactions are taken place. Note that one caveat in comparing overall intensities of one coordinate on the Kroll diagram to another is that the sensitivity may vary from species to species. As illustrated in Sect. 3.1 through our sensitivity analyses, this variation is expected to be much less for $CH_3C(O)O^-$ and $I(H_2O)_n^-$ than for $(H_2O)_nH^+$.

4 Significance and conclusions

Given the widespread use of CIMS in the atmospheric chemistry community, it is important to assess how well CIMS can be used to determine the chemical nature of aerosol composition, especially SOA (Sareen et al., 2010; Yatavelli and Thornton, 2010; Yatavelli et al., 2012; Zhao et al., 2012). In this paper, we have focussed on two aspects of this analysis, taking advantage of new instrumental advances in the field, especially a high resolution time-of-flight that can readily be deployed to the field (Bertram et al., 2011). In particular, we have addressed how the composition of a common WSOC SOA material is analyzed using three common CIMS reagent ions, monitoring both the starting material but also the changes that arise during an aqueous OH oxidation process. To our knowledge this is the first illustration of the comparative abilities of these common reagent ions to study the composition of complex organic mixtures, such as SOA. As well, while it was convenient for us to monitor change occurring during aqueous phase oxidation in the laboratory, we stress that the same

AMTD
6, 6147–6186, 2013

general behavior is likely to be observed from chemical change being driven by gas phase or heterogeneous OH oxidation. It is hoped that these characterization experiments will form the foundation for similar analyses of aging processes observed in the field as well. For example, these methods could be used for studying cloudwater oxidation (Lee et al., 2012) or atmospheric aerosol processing as observed using the MOVI interface (Yatavelli and Thornton, 2010; Yatavelli et al., 2012).

Specific findings include:

- Complex organic composition of atmospherically relevant WSOC samples can be resolved with high resolution aerosol CI-ToFMS.
- The monomer and dimer regions of α-pinene SOA WSOC can be resolved and observed with CI-ToFMS, most clearly with $I(H_2O)_n^-$ reagent ions. The chemical change of these two regions can be followed on-line with the dimers degrading more rapidly than the monomers.
- The simplicity in the switching of the CI-ToFMS reagent ions allows for a more comprehensive understanding of chemical change.
- This also illustrates that care must be taken when choosing the reagent ions with which to operate depending on the targeted analysis. For instance, $(H_2O)_nH^+$ reagent ions are shown to be more selective towards the more reduced organic compounds with WSOC SOA, while $CH_3C(O)O^-$ and $I(H_2O)_n^-$ allow for the detection of more highly oxygenated compounds with $I(H_2O)_n^-$ being more selective to multifunctional compounds. In general, the range of sensitivities for the latter two reagent ions is far less than with the more selective $(H_2O)_nH^+$.
- Despite these potential differences in sensitivity to different analytes, we point out that the data arising from a combination of the $(H_2O)_nH^+$ data and either the $CH_3C(O)O^-$ and $I(H_2O)_n^-$ results yield a van Krevelen analysis that is remarkably similar to that measured simultaneously by high resolution AMS, despite the AMS being only sensitive to particle phase species and the CI-ToFMS to both gas and

AMTD
6, 6147–6186, 2013

particle phases. Thus, the demonstrated ability of AMS data to study aging of organic aerosol using van Krevelen analysis can also be applied using CI-ToFMS data.

– Aerosol-CI-ToFMS clearly can monitor the functionalization and fragmentation processes that occur with SOA as it is oxidized by OH, generally giving rise to more functionalized products that are of lower carbon number and higher oxidation state.

– A potential source of data analysis complications is the presence of gas phase ion clusters, specifically in the cases of $(H_2O)_nH^+$ and $CH_3C(O)O^-$ reagent ions. In addition, dehydration of organics in the heated inlet or ions fragmentation in the CI-ToFMS can increase the difficulty of the identification of the unknown analyte present in the aqueous solution.

To finish, we note that the SOA aerosol-CI-ToFMS spectra also contain an enormous amount of detailed mechanistic information, related to the formation and decay of specific chemical species. An analysis of these spectra in that context will form the basis of a subsequent publication.

Supplementary material related to this article is available online at: http://www.atmos-meas-tech-discuss.net/6/6147/2013/amtd-6-6147-2013-supplement.pdf.

Acknowledgements. The authors would like to acknowledge infrastructure funding from the Canada Foundation for Innovation and Ontario Research Foundation to the Canadian Aerosol Research Network. As well, operational support comes from NSERC, OGS, Environment Canada and the Alex Harrison Award in Analytical Mass Spectrometry. The authors note extensive help from Harald Stark (Aerodyne Inc.) and Ran Zhao (Abbatt group) with the operation and data analysis of the CIMS.

AMTD
6, 6147–6186, 2013

References

Aiken, A. C., DeCarlo, P. F., and Jimenez, J. L.: Elemental analysis of organic species with electron ionization high-resolution mass spectrometry, Anal. Chem., 79, 8350–8358, 2007.

Aiken, A. C., Decarlo, P. F., Kroll, J. H., Worsnop, D. R., Huffman, J. A., Docherty, K. S., Ulbrich, I. M., Mohr, C., Kimmel, J. R., Sueper, D., Sun, Y., Zhang, Q., Trimborn, A., Northway, M., Ziemann, P. J., Canagaratna, M. R., Onasch, T. B., Alfarra, M. R., Prevot, A. S. H., Dommen, J., Duplissy, J., Metzger, A., Baltensperger, U., and Jimenez, J. L.: O/C and OM/OC ratios of primary, secondary, and ambient organic aerosols with high-resolution time-of-flight aerosol mass spectrometry, Environ. Sci. Technol., 42, 4478–4485, 2008.

Altieri, K. E., Seitzinger, S. P., Carlton, A. G., Turpin, B. J., Klein, G. C., and Marshall, A. G.: Oligomers formed through in-cloud methylglyoxal reactions: Chemical composition, properties, and mechanisms investigated by ultra-high resolution FT-ICR mass spectrometry, Atmos. Environ., 42, 1476–1490, 2008.

Bateman, A. P., Walser, M. L., Desyaterik, Y., Laskin, J., Laskin, A., and Nizkorodov, S. A.: The effect of solvent on the analysis of secondary organic aerosol using electrospray ionization mass spectrometry, Environ. Sci. Technol., 42, 7341–7346, 2008.

Bertram, T. H., Kimmel, J. R., Crisp, T. A., Ryder, O. S., Yatavelli, R. L. N., Thornton, J. A., Cubison, M. J., Gonin, M., and Worsnop, D. R.: A field-deployable, chemical ionization time-of-flight mass spectrometer, Atmos. Meas. Tech., 4, 1471–1479, doi:10.5194/amt-4-1471-2011, 2011.

Bones, D. L., Henricksen, D. K., Mang, S. A., Gonsior, M., Bateman, A. P., Nguyen, T. B., Cooper, W. J., and Nizkorodov, S. A.: Appearance of strong absorbers and fluorophores in limonene-O-3 secondary organic aerosol due to NH4+-mediated chemical aging over long time scales, J. Geophys. Res.-Atmos., 115, D05203, doi:10.1029/2009JD012864, 2010.

Caldwell, G. and Kebarle, P.: Binding-Energies and Structural Effects in Halide Anion ROH and RCOOH Complexes from Gas-Phase Equilibria Measurements, J. Am. Chem. Soc., 106, 967–969, 1984.

Canagaratna, M. R., Jayne, J. T., Jimenez, J. L., Allan, J. D., Alfarra, M. R., Zhang, Q., Onasch, T. B., Drewnick, F., Coe, H., Middlebrook, A., Delia, A., Williams, L. R., Trimborn, A. M., Northway, M. J., DeCarlo, P. F., Kolb, C. E., Davidovits, P., and Worsnop, D. R.: Chemical and microphysical characterization of ambient aerosols with the aerodyne aerosol mass spectrometer, Mass Spectrom. Rev., 26, 185–222, 2007.

AMTD
6, 6147–6186, 2013

Cleveland, M. J., Ziemba, L. D., Griffin, R. J., Dibb, J. E., Anderson, C. H., Lefer, B., and Rappenglueck, B.: Characterization of urban aerosol using aerosol mass spectrometry and proton nuclear magnetic resonance spectroscopy, Atmos. Environ., 54, 511–518, 2012.

De Gouw, J. and Jimenez, J. L.: Organic Aerosols in the Earth's Atmosphere, Environ. Sci. Technol., 43, 7614–7618, 2009.

Decesari, S., Facchini, M., Fuzzi, S., and Tagliavini, E.: Characterization of water-soluble organic compounds in atmospheric aerosol: A new approach, J. Geophys. Res.-Atmos., 105, 1481–1489, 2000.

Decesari, S., Mircea, M., Cavalli, F., Fuzzi, S., Moretti, F., Tagliavini, E., and Facchini, M. C.: Source attribution of water-soluble organic aerosol by nuclear magnetic resonance spectroscopy, Environ. Sci. Technol., 41, 2479–2484, 2007.

Decesari, S., Finessi, E., Rinaldi, M., Paglione, M., Fuzzi, S., Stephanou, E. G., Tziaras, T., Spyros, A., Ceburnis, D., O'Dowd, C., Dall'Osto, M., Harrison, R. M., Allan, J., Coe, H., and Facchini, M. C.: Primary and secondary marine organic aerosols over the North Atlantic Ocean during the MAP experiment, J. Geophys. Res.-Atmos., 116, D22210, doi:10.1029/2011JD016204, 2011.

Duarte, R. M. B. O. and Duarte, A. C.: A critical review of advanced analytical techniques for water-soluble organic matter from atmospheric aerosols, TrAC, Trends Anal. Chem., 30, 1659–1671, 2011.

Duarte, R., Pio, C., and Duarte, A.: Spectroscopic study of the water-soluble organic matter isolated from atmospheric aerosols collected under different atmospheric conditions, Anal. Chim. Acta, 530, 7–14, 2005.

Duarte, R. M. B. O., Santos, E. B. H., Pio, C. A., and Duarte, A. C.: Comparison of structural features of water-soluble organic matter from atmospheric aerosols with those of aquatic humic substances, Atmos. Environ., 41, 8100–8113, 2007.

Ervens, B., Turpin, B. J., and Weber, R. J.: Secondary organic aerosol formation in cloud droplets and aqueous particles (aqSOA): a review of laboratory, field and model studies, Atmos. Chem. Phys., 11, 11069–11102, doi:10.5194/acp-11-11069-2011, 2011.

Finessi, E., Decesari, S., Paglione, M., Giulianelli, L., Carbone, C., Gilardoni, S., Fuzzi, S., Saarikoski, S., Raatikainen, T., Hillamo, R., Allan, J., Mentel, Th. F., Tiitta, P., Laaksonen, A., Petäjä, T., Kulmala, M., Worsnop, D. R., and Facchini, M. C.: Determination of the biogenic secondary organic aerosol fraction in the boreal forest by NMR spectroscopy, Atmos. Chem. Phys., 12, 941–959, doi:10.5194/acp-12-941-2012, 2012.

AMTD
6, 6147–6186, 2013

Gard, E., Mayer, J., Morrical, B., Dienes, T., Fergenson, D., and Prather, K.: Real-time analysis of individual atmospheric aerosol particles: Design and performance of a portable ATOFMS, Anal. Chem., 69, 4083–4091, 1997.
Ge, X., Zhang, Q., Sun, Y., Ruehl, C. R., and Setyan, A.: Effect of aqueous-phase processing on aerosol chemistry and size distributions in Fresno, California, during wintertime, Environ. Chem., 9, 221–235, 2012.
Gyawali, M., Arnott, W. P., Zaveri, R. A., Song, C., Moosmüller, H., Liu, L., Mishchenko, M. I., Chen, L.-W. A., Green, M. C., Watson, J. G., and Chow, J. C.: Photoacoustic optical properties at UV, VIS, and near IR wavelengths for laboratory generated and winter time ambient urban aerosols, Atmos. Chem. Phys., 12, 2587-2601, doi:10.5194/acp-12-2587-2012, 2012.
Hallquist, M., Wenger, J. C., Baltensperger, U., Rudich, Y., Simpson, D., Claeys, M., Dommen, J., Donahue, N. M., George, C., Goldstein, A. H., Hamilton, J. F., Herrmann, H., Hoffmann, T., Iinuma, Y., Jang, M., Jenkin, M. E., Jimenez, J. L., Kiendler-Scharr, A., Maenhaut, W., McFiggans, G., Mentel, Th. F., Monod, A., Prévôt, A. S. H., Seinfeld, J. H., Surratt, J. D., Szmigielski, R., and Wildt, J.: The formation, properties and impact of secondary organic aerosol: current and emerging issues, Atmos. Chem. Phys., 9, 5155–5236, doi:10.5194/acp-9-5155-2009, 2009.
Hamilton, J. F., Webb, P. J., Lewis, A. C., Hopkins, J. R., Smith, S., and Davy, P.: Partially oxidised organic components in urban aerosol using GCXGC-TOF/MS, Atmos. Chem. Phys., 4, 1279–1290, doi:10.5194/acp-4-1279-2004, 2004.
Heald, C. L., Kroll, J. H., Jimenez, J. L., Docherty, K. S., DeCarlo, P. F., Aiken, A. C., Chen, Q., Martin, S. T., Farmer, D. K., and Artaxo, P.: A simplified description of the evolution of organic aerosol composition in the atmosphere, Geophys. Res. Lett., 37, L08803, doi:10.1029/2010GL042737, 2010.
Hearn, J. and Smith, G.: A chemical ionization mass spectrometry method for the online analysis of organic aerosols, Anal. Chem., 76, 2820–2826, 2004.
Hearn, J. D. and Smith, G. D.: Reactions and mass spectra of complex particles using Aerosol CIMS, Int. J. Mass Spectrom., 258, 95–103, 2006.
Hunter, E. and Lias, S.: Evaluated gas phase basicities and proton affinities of molecules: An update, J. Phys. Chem. Ref. Data, 27, 413–656, 1998.
Jimenez, J. L., Canagaratna, M. R., Donahue, N. M., Prevot, A. S. H., Zhang, Q., Kroll, J. H., DeCarlo, P. F., Allan, J. D., Coe, H., Ng, N. L., Aiken, A. C., Docherty, K. S., Ulbrich, I. M., Grieshop, A. P., Robinson, A. L., Duplissy, J., Smith, J. D., Wilson, K. R., Lanz, V. A., Hueglin,

AMTD
6, 6147–6186, 2013

C., Sun, Y. L., Tian, J., Laaksonen, A., Raatikainen, T., Rautiainen, J., Vaattovaara, P., Ehn, M., Kulmala, M., Tomlinson, J. M., Collins, D. R., Cubison, M. J., Dunlea, E. J., Huffman, J. A., Onasch, T. B., Alfarra, M. R., Williams, P. I., Bower, K., Kondo, Y., Schneider, J., Drewnick, F., Borrmann, S., Weimer, S., Demerjian, K., Salcedo, D., Cottrell, L., Griffin, R., Takami, A., Miyoshi, T., Hatakeyama, S., Shimono, A., Sun, J. Y., Zhang, Y. M., Dzepina, K., Kimmel, J. R., Sueper, D., Jayne, J. T., Herndon, S. C., Trimborn, A. M., Williams, L. R., Wood, E. C., Middlebrook, A. M., Kolb, C. E., Baltensperger, U., and Worsnop, D. R.: Evolution of Organic Aerosols in the Atmosphere, Science, 326, 1525–1529, 2009.

Jokinen, T., Sipilä, M., Junninen, H., Ehn, M., Lönn, G., Hakala, J., Petäjä, T., Mauldin III, R. L., Kulmala, M., and Worsnop, D. R.: Atmospheric sulphuric acid and neutral cluster measurements using CI-APi-TOF, Atmos. Chem. Phys., 12, 4117–4125, doi:10.5194/acp-12-4117-2012, 2012.

Kanakidou, M., Seinfeld, J. H., Pandis, S. N., Barnes, I., Dentener, F. J., Facchini, M. C., Van Dingenen, R., Ervens, B., Nenes, A., Nielsen, C. J., Swietlicki, E., Putaud, J. P., Balkanski, Y., Fuzzi, S., Horth, J., Moortgat, G. K., Winterhalter, R., Myhre, C. E. L., Tsigaridis, K., Vignati, E., Stephanou, E. G., and Wilson, J.: Organic aerosol and global climate modelling: a review, Atmos. Chem. Phys., 5, 1053–1123, doi:10.5194/acp-5-1053-2005, 2005.

Kroll, J. H., Smith, J. D., Che, D. L., Kessler, S. H., Worsnop, D. R., and Wilson, K. R.: Measurement of fragmentation and functionalization pathways in the heterogeneous oxidation of oxidized organic aerosol, Phys. Chem. Chem. Phys., 11, 8005–8014, 2009.

Kroll, J. H., Donahue, N. M., Jimenez, J. L., Kessler, S. H., Canagaratna, M. R., Wilson, K. R., Altieri, K. E., Mazzoleni, L. R., Wozniak, A. S., Bluhm, H., Mysak, E. R., Smith, J. D., Kolb, C. E., and Worsnop, D. R.: Carbon oxidation state as a metric for describing the chemistry of atmospheric organic aerosol, Nat. Chem., 3, 133–139, 2011.

Kundu, S., Fisseha, R., Putman, A. L., Rahn, T. A., and Mazzoleni, L. R.: High molecular weight SOA formation during limonene ozonolysis: insights from ultrahigh-resolution FT-ICR mass spectrometry characterization, Atmos. Chem. Phys., 12, 5523–5536, doi:10.5194/acp-12-5523-2012, 2012.

Laskin, A., Laskin, J., and Nizkorodov, S. A.: Mass spectrometric approaches for chemical characterisation of atmospheric aerosols: critical review of the most recent advances, Environ. Chem., 9, 163–189, 2012.

AMTD
6, 6147–6186, 2013

Laskin, J., Laskin, A., and Nizkorodov, S. A.: New mass spectrometry techniques for studying physical chemistry of atmospheric heterogeneous processes, Int. Rev. Phys. Chem., 32, 128–170, 2013.

Lee, A. K. Y., Hayden, K. L., Herckes, P., Leaitch, W. R., Liggio, J., Macdonald, A. M., and Abbatt, J. P. D.: Characterization of aerosol and cloud water at a mountain site during WACS 2010: secondary organic aerosol formation through oxidative cloud processing, Atmos. Chem. Phys., 12, 7103–7116, doi:10.5194/acp-12-7103-2012, 2012.

Lim, Y. B., Tan, Y., Perri, M. J., Seitzinger, S. P., and Turpin, B. J.: Aqueous chemistry and its role in secondary organic aerosol (SOA) formation, Atmos. Chem. Phys., 10, 10521–10539, 2010.

Mazzoleni, L. R., Ehrmann, B. M., Shen, X., Marshall, A. G., and Collett Jr., J. L.: Water-Soluble Atmospheric Organic Matter in Fog: Exact Masses and Chemical Formula Identification by Ultrahigh-Resolution Fourier Transform Ion Cyclotron Resonance Mass Spectrometry, Environ. Sci. Technol., 44, 3690–3697, 2010.

Moosmueller, H., Chakrabarty, R. K., and Arnott, W. P.: Aerosol light absorption and its measurement: A review, J. Quant. Spectrosc. Ra., 110, 844–878, 2009.

Moretti, F., Tagliavini, E., Decesari, S., Facchini, M. C., Rinaldi, M., and Fuzzi, S.: NMR determination of total carbonyls and carboxyls: A tool for tracing the evolution of atmospheric oxidized organic aerosols, Environ. Sci. Technol., 42, 4844–4849, 2008.

Murphy, D. M. and Thomson, D. S.: Laser Ionization Mass-Spectroscopy of Single Aerosol-Particles, Aerosol. Sci. Technol., 22, 237–249, 1995.

National Institute of Standards and Technology: Water, available at: http://webbook.nist.gov/cgi/cbook.cgi?ID=C7732185&Units=SI&Mask=40#Ion-Cluster, last access: 30 March 2013.

Ng, N. L., Canagaratna, M. R., Jimenez, J. L., Chhabra, P. S., Seinfeld, J. H., and Worsnop, D. R.: Changes in organic aerosol composition with aging inferred from aerosol mass spectra, Atmos. Chem. Phys., 11, 6465–6474, doi:10.5194/acp-11-6465-2011, 2011.

Onasch, T. B., Trimborn, A., Fortner, E. C., Jayne, J. T., Kok, G. L., Williams, L. R., Davidovits, P., and Worsnop, D. R.: Soot Particle Aerosol Mass Spectrometer: Development, Validation, and Initial Application, Aerosol Sci. Technol., 46, 804–817, 2012.

Perri, M. J., Seitzinger, S., and Turpin, B. J.: Secondary organic aerosol production from aqueous photooxidation of glycolaldehyde: Laboratory experiments, Atmos. Environ., 43, 1487–1497, 2009.

AMTD
6, 6147–6186, 2013

Polidori, A., Turpin, B. J., Davidson, C. I., Rodenburg, L. A., and Maimone, F.: Organic PM2.5: Fractionation by Polarity, FTIR Spectroscopy, and OM/OC Ratio for the Pittsburgh Aerosol, Aerosol Sci. Technol., 42, 233–246, 2008.

Pratt, K. A. and Prather, K. A.: Mass spectrometry of atmospheric aerosols – Recent developments and applications. Part I: Off-line mass spectrometry techniques, Mass Spectrom. Rev., 31, 1–16, 2012a.

Pratt, K. A. and Prather, K. A.: Mass spectrometry of atmospheric aerosols – Recent developments and applications. Part II: On-line mass spectrometry techniques, Mass Spectrom. Rev., 31, 17–48, 2012b.

Russell, L. M., Bahadur, R., Hawkins, L. N., Allan, J., Baumgardner, D., Quinn, P. K., and Bates, T. S.: Organic aerosol characterization by complementary measurements of chemical bonds and molecular fragments, Atmos. Environ., 43, 6100–6105, 2009.

Santos, P. S. M., Santos, E. B. H., and Duarte, A. C.: First spectroscopic study on the structural features of dissolved organic matter isolated from rainwater in different seasons, Sci. Total Environ., 426, 172–179, 2012.

Sareen, N., Schwier, A. N., Shapiro, E. L., Mitroo, D., and McNeill, V. F.: Secondary organic material formed by methylglyoxal in aqueous aerosol mimics, Atmos. Chem. Phys., 10, 997–1016, doi:10.5194/acp-10-997-2010, 2010.

Sax, M., Zenobi, R., Baltensperger, U., and Kalberer, M.: Time Resolved Infrared Spectroscopic Analysis of Aerosol Formed by Photo-Oxidation of 1,3,5-Trimethylbenzene and α-Pinene, Aerosol. Sci. Technol., 39, 822–830, 2005.

Schmitt-Kopplin, P., Gelencser, A., Dabek-Zlotorzynska, E., Kiss, G., Hertkorn, N., Harir, M., Hong, Y., and Gebefuegi, I.: Analysis of the Unresolved Organic Fraction in Atmospheric Aerosols with Ultrahigh-Resolution Mass Spectrometry and Nuclear Magnetic Resonance Spectroscopy: Organosulfates As Photochemical Smog Constituents, Anal. Chem., 82, 8017–8026, 2010.

Shakya, K. M., Place Jr., P. F., Griffin, R. J., and Talbot, R. W.: Carbonaceous content and water-soluble organic functionality of atmospheric aerosols at a semi-rural New England location, J. Geophys. Res.-Atmos., 117, D03301, doi:10.1029/2011JD016113, 2012.

Shapiro, E. L., Szprengiel, J., Sareen, N., Jen, C. N., Giordano, M. R. and McNeill, V. F.: Light-absorbing secondary organic material formed by glyoxal in aqueous aerosol mimics, Atmos. Chem. Phys., 9, 2289-2300, 2009.

AMTD
6, 6147–6186, 2013

Takahama, S., Johnson, A., and Russell, L. M.: Quantification of Carboxylic and Carbonyl Functional Groups in Organic Aerosol Infrared Absorbance Spectra, Aerosol Sci. Technol., 47, 310–325, 2013.

Tan, Y., Perri, M. J., Seitzinger, S. P., and Turpin, B. J.: Effects of Precursor Concentration and Acidic Sulfate in Aqueous Glyoxal-OH Radical Oxidation and Implications for Secondary Organic Aerosol, Environ. Sci. Technol., 43, 8105–8112, 2009.

Tan, Y., Carlton, A. G., Seitzinger, S. P., and Turpin, B. J.: SOA from methylglyoxal in clouds and wet aerosols: Measurement and prediction of key products, Atmos. Environ., 44, 5218–5226, 2010.

Thornton, J. and Abbatt, J.: N_2O_5 reaction on submicron sea salt aerosol: Kinetics, products, and the effect of surface active organics, J. Phys. Chem. A, 109, 10004–10012, 2005.

Thornton, J., Braban, C., and Abbatt, J.: N_2O_5 hydrolysis on sub-micron organic aerosols: the effect of relative humidity, particle phase, and particle size, Phys. Chem. Chem. Phys., 5, 4593–4603, 2003.

Veres, P., Roberts, J. M., Warneke, C., Welsh-Bon, D., Zahniser, M., Herndon, S., Fall, R., and de Gouw, J.: Development of negative-ion proton-transfer chemical-ionization mass spectrometry (NI-PT-CIMS) for the measurement of gas-phase organic acids in the atmosphere, Int. J. Mass Spectrom., 274, 48–55, 2008.

Wagner, R., Linke, C., Naumann, K., Schnaiter, M., Vragel, M., Gangl, M., and Horvath, H.: A review of optical measurements at the aerosol and cloud chamber AIDA, J. Quant. Spectrosc. Ra., 110, 930–949, 2009.

Walser, M. L., Park, J., Gomez, A. L., Russell, A. R., and Nizkorodov, S. A.: Photochemical aging of secondary organic aerosol particles generated from the oxidation of d-limonene, J. Phys. Chem. A, 111, 1907–1913, 2007.

Yatavelli, R. L. N. and Thornton, J. A.: Particulate Organic Matter Detection Using a Micro-Orifice Volatilization Impactor Coupled to a Chemical Ionization Mass Spectrometer (MOVI-CIMS), Aerosol Sci. Technol., 44, 61–74, 2010.

Yatavelli, R. L. N., Lopez-Hilfiker, F., Wargo, J. D., Kimmel, J. R., Cubison, M. J., Bertram, T. H., Jimenez, J. L., Gonin, M., Worsnop, D. R., and Thornton, J. A.: A Chemical Ionization High-Resolution Time-of-Flight Mass Spectrometer Coupled to a Micro Orifice Volatilization Impactor (MOVI-HRToF-CIMS) for Analysis of Gas and Particle-Phase Organic Species, Aerosol Sci. Technol., 46, 1313–1327, 2012.

AMTD
6, 6147–6186, 2013

Zhang, Q., Jimenez, J. L., Canagaratna, M. R., Allan, J. D., Coe, H., Ulbrich, I., Alfarra, M. R., Takami, A., Middlebrook, A. M., Sun, Y. L., Dzepina, K., Dunlea, E., Docherty, K., DeCarlo, P. F., Salcedo, D., Onasch, T., Jayne, J. T., Miyoshi, T., Shimono, A., Hatakeyama, S., Takegawa, N., Kondo, Y., Schneider, J., Drewnick, F., Borrmann, S., Weimer, S., Demerjian, K., Williams, P., Bower, K., Bahreini, R., Cottrell, L., Griffin, R. J., Rautiainen, J., Sun, J. Y., Zhang, Y. M., and Worsnop, D. R.: Ubiquity and dominance of oxygenated species in organic aerosols in anthropogenically-influenced Northern Hemisphere midlatitudes, Geophys. Res. Lett., 34, L13801, doi:10.1029/2007GL029979, 2007.

Zhao, R., Lee, A. K. Y., and Abbatt, J. P. D.: Investigation of Aqueous-Phase Photooxidation of Glyoxal and Methylglyoxal by Aerosol Chemical Ionization Mass Spectrometry: Observation of Hydroxyhydroperoxide Formation, J. Phys. Chem. A, 116, 6253–6263, 2012.

AMTD
6, 6147–6186, 2013

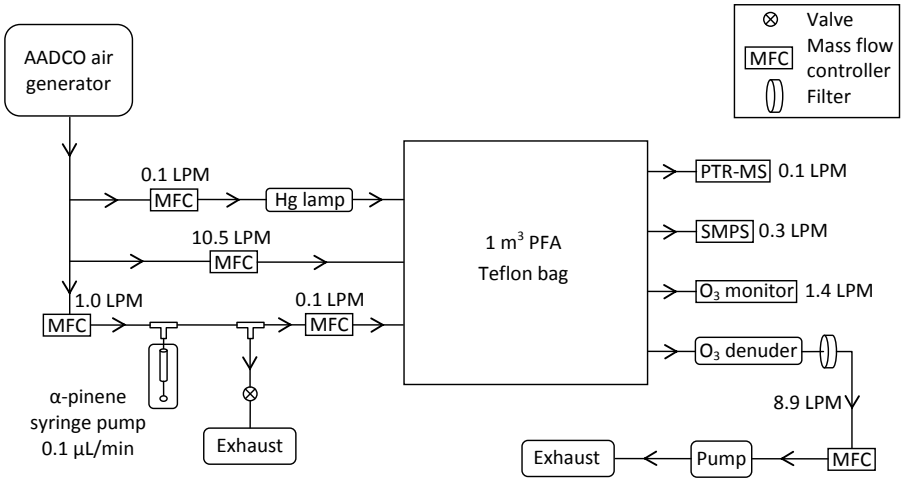

Fig. 1. Experimental set up used to run a 1 m^3 MOCA chamber in continuous mode to generate SOA by the gas phase ozonolysis of α-pinene. Air flowing into and out of the chamber was controlled by mass flow controllers. Instruments connected to the outlet of the chamber were used to monitor gas phase and particle concentrations.

AMTD
6, 6147–6186, 2013

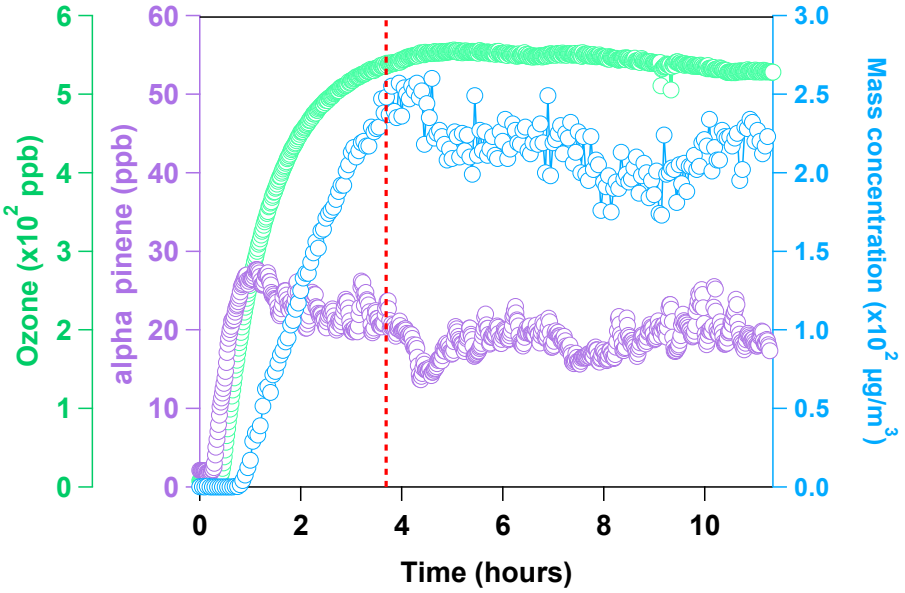

Fig. 2. Time profiles of O_3, α-pinene and SOA mass loading evolution in the MOCA chamber, which was run in continuous mode. Dashed red line indicates when SOA collection started.

AMTD
6, 6147–6186, 2013

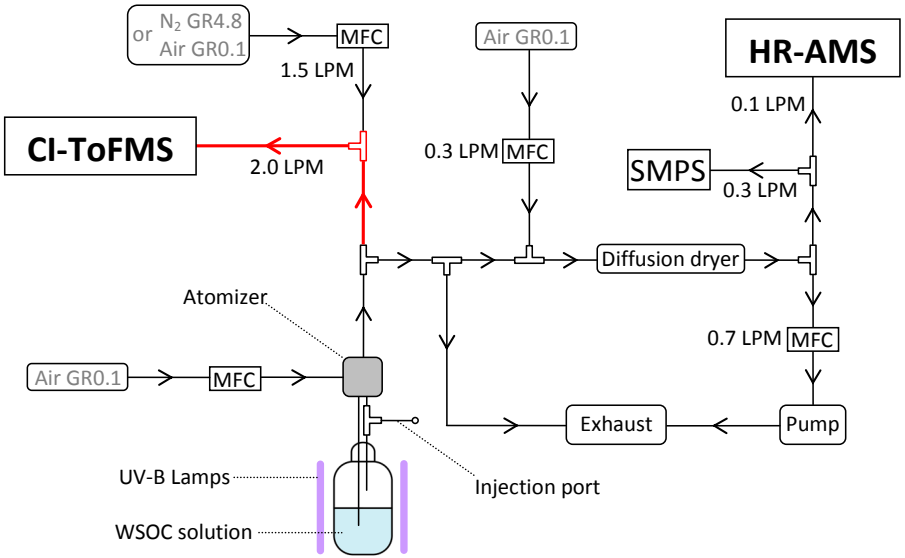

Fig. 3. Setup used to run the aqueous phase photo-oxidation of WSOC. The solution was constantly stirred and atomized in the glass bottle while UV-B light was continuously irradiated for 4 h. The flow carrying the mist from the atomizer was split such that part was introduced to the HR CI-ToFMS and the rest was admitted to the HR-AMS and SMPS. Red line indicates the CI-ToFMS heated inlet (150 °C). MFC refers to mass flow controller.

AMTD
6, 6147–6186, 2013

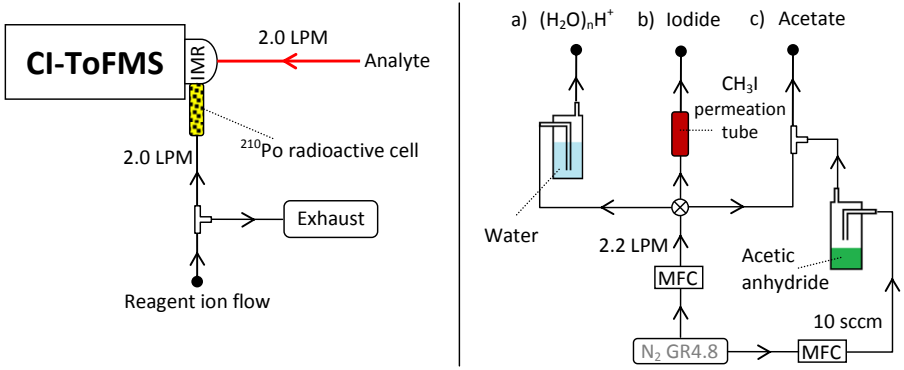

Fig. 4. The setup used to operate the CI-ToFMS. Sample flow was introduced to the IMR through the heated inlet. $(H_2O)_nH^+$, $I(H_2O)_n$ and acetate reagent ions were generated by passing a flow of nitrogen gas carrying (a) water (b) methyl iodide and (c) acetic anhydride through a ^{210}Po radioactive cell, respectively. One reagent ion was used at a time. Bolded circles indicate points of attachment of the reagent ion flows on the right to the manifold on the left. Sccm refers to Standard Cubic Centimeters per Minute.

AMTD
6, 6147–6186, 2013

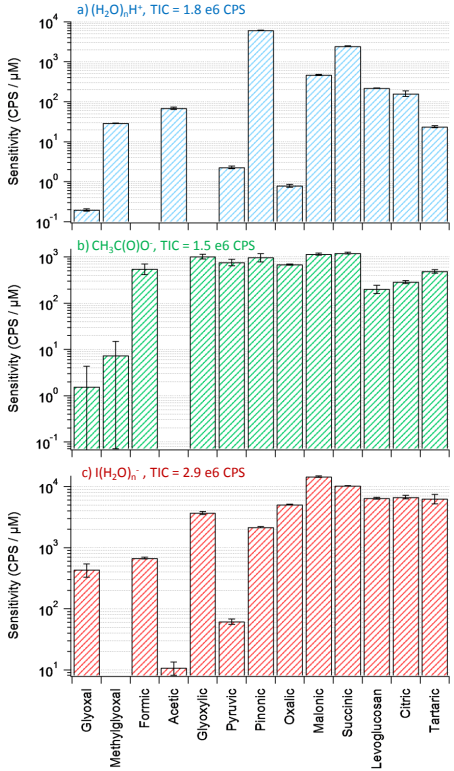

Fig. 5. The sensitivity of 13 organic compounds in units of CPS (counts per second)/µM in solution. The sensitivities were obtained by operating the CI-ToFMS with the three reagent ions **(a)** $(H_2O)_nH^+$, giving rise to protonated molecular ions, **(b)** $CH_3C(O)O^-$, giving rise to deprotonated species aside from levoglucasan which was detected as a cluster with acetate, and **(c)** $I(H_2O)_n^-$, giving rise to clusters with iodide. The error bars reflect the standard error in the slopes of the 3-point calibration curves. Also, the total ion count (TIC) is shown for each reagent ion.

AMTD
6, 6147–6186, 2013

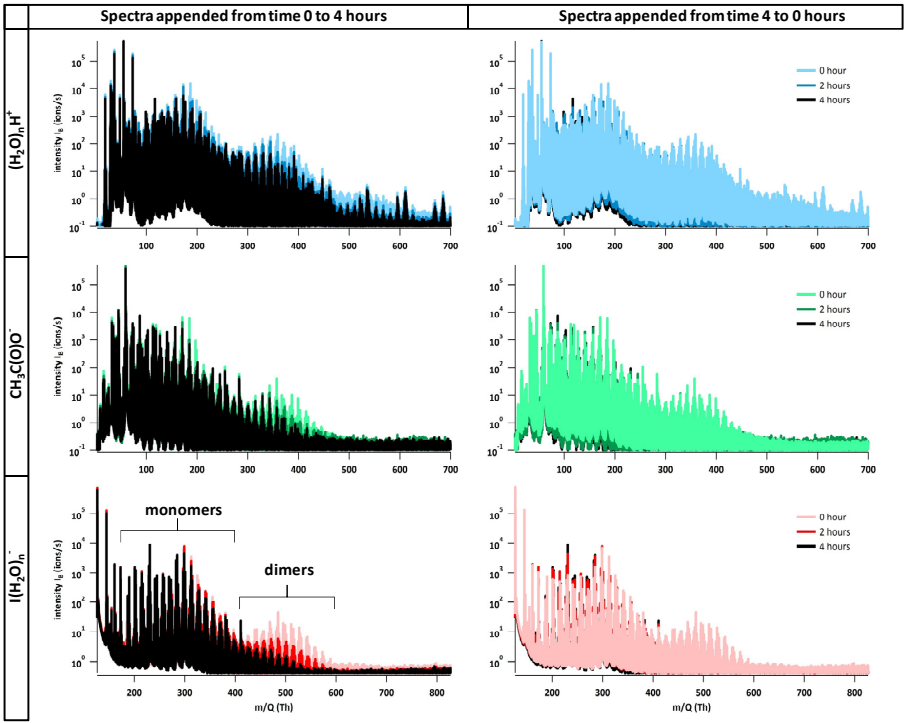

Fig. 6. Mass spectra of the photo-oxidized SOA using the three reagent ions, protonated water clusters $(H_2O)_nH^+$, acetate $CH_3C(O)O^-$ and iodide water clusters $I(H_2O)_n^-$, at time 0, 2 and 4 h. The spectra on the left show the *m/z* regions where the intensity decreased indicating loss of signal. The spectra on the right show the m/z regions where the intensity increased for some ions illustrating products formation. Monomer and dimer regions were observed in the spectra of the three reagent ions, most clearly in the $I(H_2O)_n$ spectra.

AMTD
6, 6147–6186, 2013

Focus on formation of oxygenated species via aqueous phase processing

D. Aljawhary et al.

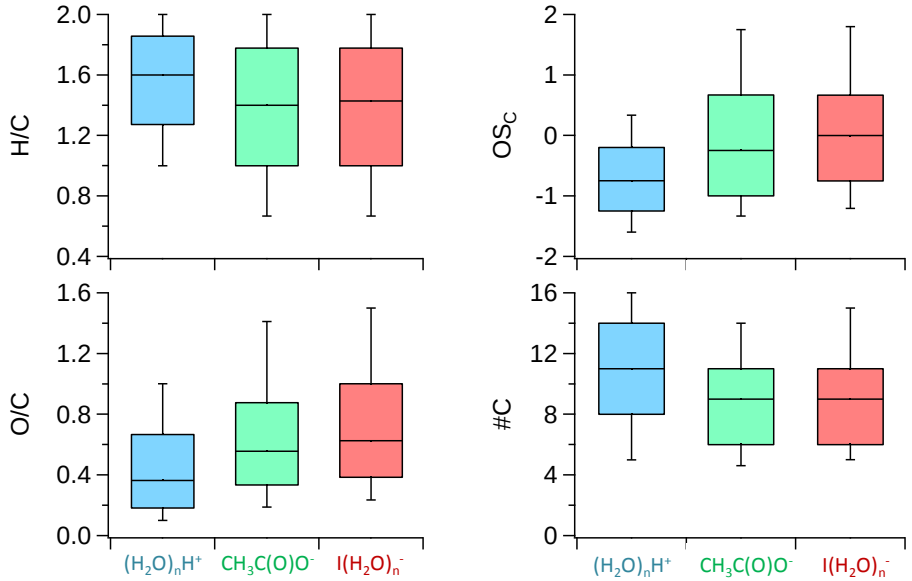

Fig. 7. Box plots showing the 10th, 25th, 50th, 75th and 90th percentiles for H/C, OC, OS_C and #C for the pool of ions detected by each reagent ion. The population size was 595, 555 and 428 ions for $(H_2O)_nH^+$, $CH_3C(O)O^-$ and $I(H_2O)_n^-$, respectively.

AMTD
6, 6147–6186, 2013

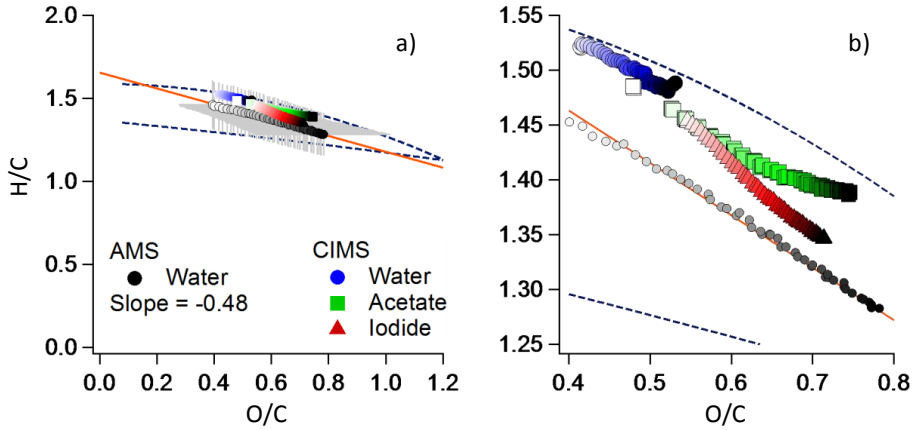

Fig. 8. Van Krevelen diagram of the AMS and CI-ToFMS data for the WSOC aqueous phase photo-oxidation using the three reagent ions. The plot on the right is an expanded view of the plot on the left. The time scale covers the 4 h of photo-oxidation moving from light to dark bolded symbols. The dark blue dashed lines are the parameterized O/C and H/C from the triangle plot compiling a large dataset of ambient and laboratory data as described in (Ng et al., 2011). Note that although AMS measurements were conducted for each experiment, for clarity sake only one set of data is plotted here; the other experiments gave similar results. The linear fit for the AMS data, which is shown in orange, had a slope of −0.48. The error bars of the AMS H/C and O/C are shown in gray obtained from the H/C and O/C accuracies of 10 % and 30 % reported in (Aiken et al., 2007).

AMTD
6, 6147–6186, 2013

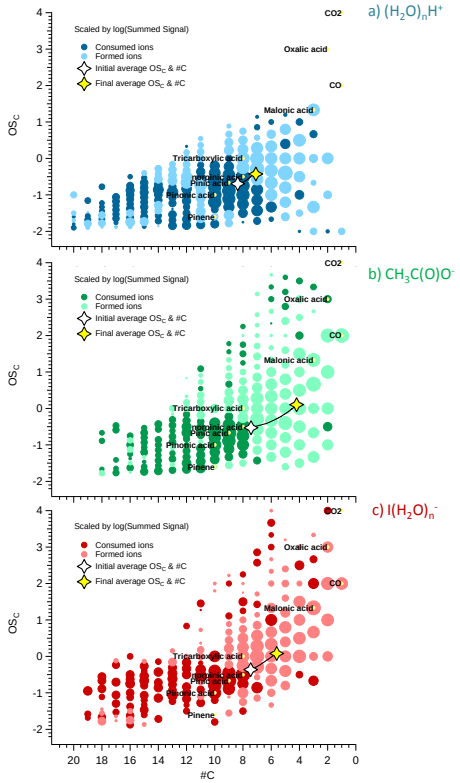

Fig. 9. Difference Kroll diagrams for the WSOC before oxidation and after 4 h of oxidation using the three reagent ions; $(H_2O)_nH^+$, $CH_3C(O)O^-$ and $I(H_2O)_n^-$. Light bolded circles indicate coordinates where ions formed while dark bolded circles indicate ion losses. The average OS_C and #C are also shown over 4 h of oxidation. The size of marker indicates the magnitude of the subtracted intensity.

AMTD
6, 6147–6186, 2013